Advanced Engineering Materials **4**(10), 814–823 (2002)

# Process control in aluminium foam production using real-time x-ray radioscopy

**Heiko Stanzick, Manfred Wichmann,** and **Jörg Weise**
Fraunhofer-Institute for Advanced Materials, Bremen, Germany
**Lukas Helfen** and **Tilo Baumbach**
Fraunhofer-Institute for Non-destructive Testing, Dresden, Germany
**John Banhart***
Hahn-Meitner-Institute, Berlin, Germany
* corresponding author (e-mail: banhart@hmi.de).

## Abstract

Aluminium alloy foams were created by expanding foamable precursors containing a gas releasing blowing agent in a dense metallic matrix. The precursors were prepared by two different ways: either by hot-compaction of powder mixtures or by thixo-casting of billets obtained by cold compaction of powder blends. Foam evolution was visualized by means of real-time x-ray radioscopy with image frequencies ranging up to 18 Hz and spatial resolutions down to 10 μm. The difference in pore formation between the two processing routes could be studied. Rupture of cell walls during foam expansion could be visualised, a critical rupture thickness measured and the time-scale of the rupture process estimated. By manufacturing foam precursors in which defects were incorporated deliberately, the question of the origin of very large pores in solid metal foams could be discussed. By forced cooling of liquid metal foams while recording their structure, the importance of solidification-induced changes of foam morphology was illustrated.

## 1 Introduction

Metallic foams have been causing a rise in interest in academia and industry as energy consumption reduction programmes and safety regulations are becoming increasingly stricter **[1]-[4]**. One manufacturing method for producing closed-cell metal foams **[5]-[7]** has gained especial importance because it allows for processing a wide range of materials and component geometries. The process consists of first making a foamable precursor, e.g. by mixing powdered metals, alloys or metal powder blends with a powdered blowing agent and compacting the mix to a dense semi-finished product by hot pressing, extrusion, powder rolling or some other method. In a final step, this densified precursor material is foamed by heating it up to its melting point. This softens the metal and simultaneously forces the blowing agent to decompose and to release gas, thus forming bubbles in the semi-molten metal and creating a highly porous structure. Alternative routes for preparing the foamable precursor vary the way the powder mix is densified or even start from the molten metal **[8][9]**. In all cases titanium hydride ($TiH_2$) is the preferred blowing agent for aluminium alloys. $TiH_2$ releases hydrogen gas already at 400°C, but the main decomposition takes place above 550°C.

While metal foams have been characterised thoroughly with respect to their morphology, mechanical properties and other materials properties relevant for potential applications, the actual foaming process, i.e. the process during which the foam emerges from the liquid, the way how it changes with time and the mechanisms responsible for its formation, have been studied only quite recently **[10][11]**. The use of x-ray radioscopy which allows to obtain real-time images of expanding metal foams with a high spatial and time resolution was another recent milestone **[12][13]**. In this paper we study the foaming

behaviour of aluminium alloy foams using x-ray radioscopy and discuss the following questions or phenomena closely related to applications of these materials, namely:

- Influence of precursor processing route: beside the "traditional" powder route for making metal foams an alternative method based on thixotropic moulding of pre-compacted powder mixtures was tested. The aim was to describe the difference in their foaming behaviour qualitatively,
- rupture phenomena: the ongoing gas evolution from the blowing agent and thermal expansion stretches films between adjacent bubbles and leads to sudden rupture in many cases. The obvious result is that foam morphology gets coarser with time which clearly is an unwanted effect. The goal was to determine the critical thickness of cell walls at the moment of rupture. While this quantity has been determined by ex-situ analysis of foams in the past for various alloys, we derive it from in-situ data in this paper and obtain an estimate for the rupture time of cell walls,
- defect formation: solid metal foams usually exhibit cells of all different sizes. Two different reasons for this can be assumed: due to the statistical character of foaming implying, e.g., sudden film ruptures, a certain spectrum of bubble sizes has to be expected. Furthermore, heterogeneities in the foamable precursor and temperature gradients during foaming could lead to large-scale non-uniformities in the foam. We deliberately prepare defects in the precursor and observe the pore formation near these hoping to be able to verify such effects,
- phenomena during solidification of foams: solid aluminium foams often exhibit cells which strongly deviate from a spherical or an equiaxed polyhedral shape. It is not clear whether such shapes are already present in the liquid state or whether they are created during solidification of the foam. We therefore quench a liquid foam inside the furnace while observing it by means of x-ray radioscopy.

## 2 Preparation of metal foam precursor

Metal foam was generated by two alternative methods. In both cases a foamable precursor was manufactured consisting of a dense alloy in which $TiH_2$ blowing agent particles are uniformly dispersed, but the way the precursor is made is varied (**Figure 1**).

In the first case (*route I*) the precursor was obtained by mixing aluminium powder (Al99.74, <160 μm) with silicon powder (<100 μm) in a weight ratio 93:7. To this mix 0.5 wt.% titanium hydride ($TiH_2$) powder were admixed, yielding a final composition AlSi7 + 0.5wt.% $TiH_2$. 50 kg of the powder mix were first compacted to cylindrical billets of 70 to 80% theoretical density by cold isostatic pressing (CIP) at Schunk Sintermetalltechnik GmbH (Gießen, Germany) **[7][10]**. These billets were then pre-heated to temperatures between 350 to 400°C and extruded to rectangular bars of 160×20 $mm^2$ cross-section in a second step in which the horizontal 25 MN direct extrusion machine at Honsel AG, Meschede (Germany) was used. Alternatively, the powder mix was compacted uniaxially at 450°C and 120 MPa, whenever the experimental situation called for a small batch of samples. The resulting precursor material is more than 99% dense in both cases and exhibits the anisotropies typical for a directional compaction process.

In the second case (*route II*) Al, Si, Cu and $TiH_2$ powders were mixed in fractions which led to a final alloy composition AlSi6Cu4 + 0.5wt.% $TiH_2$. The mix was first densified by cold isostatic pressing at 150 MPa. The resulting billets were then heated for 40 minutes at 590°C in an annealing furnace. After that the material showed thixotropic behaviour. The billets were manually transferred into the sleeve of a horizontal cold chamber high pressure die casting machine (locking force 6615kN) and pressed into the die cavity. The metal front velocity during the filling was approximately 1 m/s and the secondary compression pressure 190 MPa. In this way complex formed components with a uniform distribution of the blowing

agent powder and a homogeneous and mainly isotropic structure could be obtained. Samples for radioscopy were cut out of such cast components. Processing route II is in some aspects similar to other casting-oriented approaches for the production of foamable material such as, e.g., by addition of the blowing agent into the melt shortly before or during the die filling in high pressure die casting **[8]** or the admixture of specially pre-treated $TiH_2$ to a MMC melt **[9]**. In distinction to these approaches the process presented here features mixing of the metal and blowing agent in the solid state at room temperature thus facilitating a homogeneous distribution and defined initial state of the blowing agent in the precursor material and avoiding thermal treatment of the blowing agent during mixing which could lead to partial dehydrogenation.

In both cases – route I and II - the foamable precursor was converted into a foam by heating it to its melting temperature inside the furnace designed for the radioscopic measurements.

## 3 Radioscopic measurements

For the experiments the furnace was pre-heated to a given temperature. The foamable sample was placed onto a sample holder which was open in the direction of the beam and lowered into the furnace by means of a motor-driven transfer bar. X-ray monitoring was started about 2 minutes later when the foaming process was expected to commence as the sample temperature approached the melting point.

The foaming furnace was equipped with two water-cooled Al windows through which a synchrotron x-ray beam could pass (see **Figure 2**). The beam, mono-chromatised to about 33 keV and having a cross-section of 40×15 $mm^2$, generated an absorption radiograph on a $GdO_2S$:Tb polycrystalline powder screen which converted the x-rays into light. The image was captured by an optical system and finally on either a 1024 x 1024 or a 2048 x 2048 pixel CCD camera with 19 or 14 μm pixel size, respectively. Depending on the optics used one CCD pixel corresponded to a sample area of 10, 30 or 40 μm squared. The CCD camera was read out every 500 ms in the standard operation mode. The entire foaming process took a few minutes, corresponding to a few hundred radiographs for each individual experiment.

Conventional slow scan CCDs provide a high dynamic range (16 bit) but their read-out time is usually long. The ESRF Frelon 2000 camera provides an exposure mode dedicated for achieving high frame rates with a reduced image size but conserving the dynamic range. Using this operation mode, a region of the CCD can be reserved for image exposure, the remaining surface which is not exposed serves as image storage. After exposure of the reserved part of the CCD the electric charge can then be shifted quickly to the shaded region dedicated for image storage. In this way, a fast series of images (usually 2,4,8,...) can be acquired and stocked on the CCD. The achievable maximum frequency depends on the exposure time needed for one image and the shift time which is approximately proportional to the number of detector lines used for one image. We realised by this mode exposure times in the order of 50 ms and a vertical image size of 256 lines (and 2048 pixel horizontal width) translating into a shift time of about 5 ms. Four images were accumulated on the CCD before read-out which allowed to obtain maximum frame rates of up to 18 Hz between the frames stocked on the CCD. The mean overall frame rate is limited by the CCD read-out (240 ms) to 2.2 Hz in this case.

## 4 Results and discussion

### 4.1 General foaming behaviour

Foaming behaviour depends largely on the alloy used, the processing route applied to make the precursor (in our case die-pressing, extrusion or thixocasting), the foaming

temperature [10] and some other parameters such as the ambient atmosphere and pressure **[14]** which, however, were not varied in this study. Here we compare the different processing routes available for making precursor from metal powders and restrict ourselves to casting alloys.

The main difference between the various routes is the directionality of foaming. Die-pressing and extrusion of powder mixtures creates an anisotropic microstructure. The powder particles are deformed - most visible in extruded powders - and appear elongated in micrographs. More important, bonding between powder particles is not isotropic and the strength of the consolidated powder is higher perpendicular to the compression axes. Die-pressing is uniaxial, whereas extrusion can range between uniaxial and biaxial, depending on the aspect ratio of the extruded product. As we press powders to rectangular sections of 160×20 $mm^2$, pressing is almost uniaxial in this case. However, when pressing round rods one would encounter true bi-axiality.

This anisotropy becomes visible during the early stage of foaming. The initial expansion for Al-based casting alloys takes place in the solid state for Al-based casting alloys because hydrogen already evolves below the solidification temperature and is therefore anisotropic: expansion occurs parallel to the direction of powder compaction and early pores are not round but crack-like. This can be visualised by x-ray radioscopy if x-ray beam and expansion direction are perpendicular [12] and also by computed micro-tomography **[15]**. Uniaxially pressed powders seem to exhibit a more pronounced directionality compared to extruded bars, which could be a consequence of the minor compaction axis during extrusion, but this finding still has to be further examined. Precursor material manufactured by route II, however, shows a completely different behaviour. As casting creates a largely uniform microstructure, no directional expansion is observed. Although expansion also commences in the solid state, pores are round at all times. **Figure 3** shows this difference by comparing two foams which were made from die-pressed powders and thixo-cast powder mixtures.

Analysis of fully expanded foams reveals that thixo-cast precursor leads to very uniform structures with a narrow cell size distribution and very few large and irregular pores. These are quite frequent in foams made from die-pressed powders (route I), especially if manufactured in large moulds. Although most of the crack-like initial pores observed in route-I-foams round off in the main expansion phase which takes place in the liquid state [10], some seem to lead to the dreaded "monster pores" that make the resulting solid foam useless for application engineers. Recent work carried out by the Karmann GmbH (Osnabrück) has shown that by carefully controlling the impurities in the precursor, by modifying the blowing agent and by avoiding temperature gradients during foaming, a more uniform pore structure can be obtained even when making precursors by consolidating powders in the solid state **[16]**. Therefore, it might be too early to conclude that the powder compaction method is inferior to the thixocasting route, although the latter has certain advantages.

### 4.2 Minimum thickness of cell walls

In order to determine the minimum thickness of cell walls before rupture various radioscopic image series were analysed which were taken with the highest available spatial resolution (10 μm). Some clearly visible rupture events were selected and the last image before rupture was identified. **Figure 4a** shows such a rupture event. The thickness of the rupturing cell wall in question was determined by counting the number of pixels across the thinnest section of the cell wall in the direction perpendicular to the wall, taking account of the angle between cell wall and image boundary (**Figure 4b**). As the resolution of the camera is limited the edge of the cell walls was not always sharply defined giving rise to an uncertainty of the order of one pixel on each side.

**Table 1** lists the results of these measurements for two different alloys, each one based on one of the two precursor manufacturing routes. For each sample 10 events were selected. The mean value of all these individual measurements is about the same in both cases, namely about 50 μm. This corresponds well with an earlier estimate derived from lower resolution pictures [12], where a range 50-80 μm could be estimated. The results are largely independent of the manufacturing route - I or II. The minimum cell wall thickness of Al-based foams has also been determined by other authors by analysing solid foams. **Table 2** gives such values for different alloys ordered according to their silicon content. Obviously, most alloys containing silicon have minimum wall thicknesses between 50 and 80 μm, the large scatter originating from different definitions for wall thickness and probably also a real scatter of this quantity. Pure Al has a slightly higher minimum thickness and about the same value was found for wrought alloys such as AA6061 alloys **[20]**. The origin for these lower limits is still not known. A possible reason could be the high surface tension of liquid metals which destabilises thin films much more than it is the case in aqueous foams where the surface tension is one order of magnitude lower. Moreover, solid particles within the molten metal, e.g. oxides or solid constituents of the alloy itself could cause instabilities in the cell wall and trigger rupture processes. Silicon reduces the minimum thickness compared to low-silicon alloys by 20% but the effect seems to saturate out at some wt.% of Si.

For applications one would like to further reduce the minimum thickness beyond this limit because this would mean that more cell walls survived during foam expansion and a foam with smaller cells at the same density could be obtained. This would imply better mechanical properties and better predictability of foam properties. At the moment, however, no strategy is known for achieving this goal.

### 4.3 Time of rupture processes

Rupture phenomena in unstable aqueous foams are known to occur on a very short timescale i.e. microseconds, while in metal foams these times are still unknown. A crude estimate of the time between the first instability and the disappearance of a cell wall can be obtained by using values for the surface tension of the liquid metal and rough estimates for the geometrical extensions of bubbles. Suppose that a film between two adjacent bubbles has a quadratic cross section b × b and constant thickness c (**Figure 5**). Assume that rupture takes place along a line separating the film into two equal parts. Surface tension σ will create a force F = σ × b pulling the separated halves into the remaining liquid. Let x(t) be the co-ordinate denoting the actual remaining height of the lower cell wall half. The mass of the cell wall at a given time then is m(t) = ρbcx(t), where ρ is the density of the liquid, and it is accelerated with a(t) = F/m(t) = σ/(ρcx). Therefore, as dx = -a(t)t dt, a simple integration over x=b/2...0 and t=0...T yields the time T after which the film has disappeared:

$$T = \frac{b}{2}\sqrt{\frac{c\rho}{\sigma}} = 1.2 \text{ ms}; \quad \text{using b=5 mm, c=80 μm, } \rho\text{=2400 kg/m}^3\text{, } \sigma\text{=0.87 N/m [21]}$$

This estimate does not take into account the viscosity of the liquid and that the surface of each film might be covered by a solid oxide layer which would largely delay the collapse process. In an extreme case this was observed near the surface of a freely expanding foam when collapse took several seconds [12]. For aqueous foams σ is less than 1/10 of the metal value but c can easily be in the range of 50 nm or even less, thus making T much shorter.

In a previous investigation it could be shown that in aluminium and zinc foams rupture takes place in less than 333 ms for films inside the foam where they are not exposed to air directly [12]. To obtain an improved estimate for metal foams a series of radioscopic images of an expanding AlSi6Cu4 foam (III-92, route II) at 775°C furnace temperature was taken at high repetition frequencies. This foam is particularly prone to film rupture especially at the high temperatures applied. By using the technique described in Sec. 3 we could record series

of 4 images, each separated by a time interval of 55 ms (exposure time 50 ms, time for image shift 5 ms). Several rupture events shown in these image series could be identified. It was seen that in no case an intermediate stage of a rupture was recorded. This proves that rupture takes place in less than 55 ms in this particular alloy. Taking the result of our rough calculation it can be concluded that rupture of metal foam films probably occurs on the time-scale of several milliseconds instead of microseconds as in aqueous foams. However, faster measurements are still necessary to obtain a more definite value.

### 4.4 Defects in foamable precursors and foaming of granulated precursor

*Sample preparation*

In order to learn more about the formation of large irregularities in metal foams, precursor material was prepared which contained defects or inclusions. The powder compacts were prepared by axial die-pressing in a cylindrical die of 32 mm diameter at T=450°C. One third of the total amount of the powder mix (AlSi7 + 0.5 wt.% $TiH_2$) was first filled into the die after which the defect was placed onto the powder in the centre. After this the remaining powder was carefully filled into the die and the compaction process was started. From the resulting cylindrical tablet a cuboid sample ($30\times4\times10$ mm$^3$) was EDM-machined out ensuring that the defect remained in the sample centre. The specimens were then foamed with the furnace set to 725°C (700°C for case e). Defects induced by the following inclusions were observed:

a) *mica* which is a lamellar silicate (mainly $SiO_2$ and $Al_2O_3$). A platelet $3\times3\times0.4$ mm$^3$ was used,
b) *carbon fibre* mesh, fibre cross section $800\times200$ μm$^2$, spacing between fibres 5 mm,
c) *lead oxide* powder (PbO). This offers an excellent absorption contrast due to the high x-ray absorption of lead. Moreover, such oxides inevitably lead to a lack of bonding in the Al powder,
d) M2 *steel* flat washer, outer diameter 4.75 mm.
e) two *holes* (d=2.5 mm and 5 mm) were drilled into the precursor (one parallel, one perpendicular to the beam)

A question of practical importance is whether in the production process of shaped metal foam parts a single piece of precursor is needed to obtain good foam quality or whether various pieces or even granular precursor material can be used. *Alulight Co.* (Ranshofen) has been producing Al foam panels using many individual pieces of foamable precursor wires which were arranged in parallel in the mould **[22]**. The characteristic pattern of lighter and darker greyish colours on the surface of these panels has fascinated artists and has shown that it is possible to proceed in this way, although the impact of this technique on mechanical properties has not been reported. Therefore, one more foaming situation was considered in the x-ray study, namely,

f) *granulate* of precursor material: small pieces of precursor (cuboids about 5 mm long) were cut off a larger piece of precursor and were filled into a mould (10 mm deep in the beam direction).

The following results were obtained:

*a) mica*

The mica platelet cannot be seen directly in the pictures (**Figure 6a**) but the formation of a long oblate pore at the position of the mica inclusion is obvious. In the image shown this oblate pore has about the same size as the entire mica platelet. Later images (not displayed) show that this pore does not increase in size any further. As other bubbles grow to the same size there is no difference any more between this defect-induced pore and the "natural" ones.

*b) carbon fibres*

As for the mica platelet a crack is formed at the location of the fibres. Because the fibres extend over the entire sample width this crack is correspondingly wider (**Figure 6b**). As for the mica platelet the void induced by the fibre looses significance as other bubbles are created. However, in the vicinity of the fibres local density is increased and even in much later foaming stages a region of increased density along the fibres can be detected.

*c) lead oxide*

The lead oxide traces can be easily seen due to their high x-ray absorption (**Figure 6c**). The defect is not exactly horizontal and slightly off the sample centre. A big oblate pore develops before foaming at other locations even starts (2$^{nd}$ image). Possibly lead oxide is partially or entirely reduced to metallic lead by the aluminium matrix for the high temperatures employed during foaming, but we shall continue to speak of "oxides". In the further course of foaming (not shown) the pore grows and the lead oxide layer splits, each part adhering to one inner wall of a pore. However, as foaming proceeds and bubbles grow everywhere in the sample the situation becomes less clear. In the fully expanded state some very big cells can be distinguished, but they are not unambiguously associated to the lead oxide trace any more. What can be seen around the lead oxide trace is a slight increase in density, similar to the situation with the fibres (b).

*d) steel flat washer*

The annular flat washer is clearly visible near the sample centre (**Figure 6d**). Continued heating leads to the formation of a void around the ring but this does not exclusively happen there but also at other locations in the sample. Apparently enough bonding has developed during powder compaction to prevent the formation of a very large crack. Another foaming experiment shows that ongoing foaming does not change the situation: the washer floats freely in the aluminium foam. No change in local density or pore size is observed around the steel ring.

*e) holes*

The two holes can be seen in the first image (**Figure 6e**) showing the state before foaming. The hole perpendicular to the beam (5 mm diameter) can be merely seen as grey shadow as the thickness of the original precursor in the beam direction (10 mm) is reduced around the hole. Foaming leads to a gradual closure of both holes as their inner walls expand towards the axis of each hole. However, one notices that there is a density increase near the location of each hole which remains visible even at later times, e.g. as shown in image #177. The reason for this might be oxides or traces of oil remnants from drilling which contaminate the inner surfaces of the holes and which impede foam expansion locally.

*f) granulate*

The x-ray images corresponding to various stages of granulate foaming are shown in **Figure 7**. The individual pieces (seen in image #6) first start to foam individually (#88) until they touch and amalgamate to a bigger lump of foam (#129). The final foaming stage observed (#396) shows a largely uniform foam with just some slight density-increased regions (one marked by an arrow) where two granuli possibly did not merge perfectly. These density increased regions might be similar to the ones seen in **Figure 6**e and could be explained by surface oxides or other contaminations.

In conclusion the defects which were deliberately created in the foamable precursor material do lead to local formation of big voids especially if the defects are non-metallic. However, these voids did not lead to the expected big pores in the fully expanded foam. A

slight density increase around the defects seems to be the only consequence in most cases. Density increases are also caused by contaminated internal surfaces as seen in the case of holes in the precursor and the granulate foaming experiment.

### 4.5 Effects of foam solidification

In various experiments aluminium foam formation was stopped by freezing the liquid foam during x-ray observation. For this pressurised cold air was directed towards the mould containing the expanding foam while still being inside the furnace and in the x-ray beam. Cooling could be initialised by opening a magnetic valve and the effect of cooling was monitored by a thermocouple attached to the mould.

The results of an experiment carried out on an AlSi7 foam with the furnace temperature set to T=725°C will be discussed. The mould consisted of a steel frame with two titanium sheets (thickness 0.35 mm) as face sheets. The inner dimensions of the mould were $30.15\times15.35\times10$ mm$^3$, where the latter length is traversed by the beam. The temperature as a function of time was measured with a thermocouple attached to the mould and is displayed in **Figure 8**. Prominent features are the initial rise of temperature after the mould including the precursor was lowered into the pre-heated furnace. As the eutectic temperature of the alloy at T=577°C is reached the components Al and Si amalgamate and form a liquid phase. After some time at this temperature, T rises again and passes the liquidification temperature at 620°C until the pressurised air is turned on after T=650°C has been reached. The onset of air cooling caused a slight disturbance in the corresponding x-ray pictures and can therefore be perceived very precisely in the image series. The corresponding drop of temperature is delayed by about 3s due to the thermal inertia of the mould. The temperature reaches the solidification point – 577°C – of the alloy 31 seconds after the air cooling has been turned on.

Three stages of foam expansion are shown in **Figure 9**: the first image shows the still rising foam at T=622°C. The foaming front is not a plane but vaulted. The expanding foam touches the upper side of the mould in the middle first and then flows towards the corners (not shown). The second image was taken 5 s after the onset of cooling as the temperature of the mould just starts to drop. The mould is completely filled with the liquid aluminium foam. The third image shows the foam shortly after solidification (T=572°C). One notices that the foam in the corners has receded from the mould walls, i.e. local collapse has created voids. Moreover, changes in morphology of the foam can be noticed but this effect is not very pronounced.

It is interesting to compare radioscopic images with micrographs of a corresponding foam section. This became possible in this experiment, because the sample could be preserved after cooling. **Figure 9b** shows a section which represents the central plane of the sample, i.e. the 10 mm thick foam was cut into two equal parts. At first glance there is little similarity between the pictures because the in the radiograph all features along the beam are superimposed but careful comparison allows to identify common features such as the ones marked by circles. The total height of the section is a bit lower than the radioscopic image because the top of the foam had collapsed slightly in the middle.

In order to visualise the changes of the foam after the onset of cooling difference images $\Delta i$ = image (i+1) – image(i) were calculated for the entire solidification interval. Such difference pictures allow to identify the features changing from one frame to another easily (see **Figure 4**). Where ever a rupture event was recorded it was included in the “rupture map” shown in **Figure 9c**. Clearly, the most events were recorded in the first 1.5 seconds after the onset of cooling with 24 events per second. A cluster of such events is marked by an arrow. This cluster can be identified in **Figure 9a**, #299, where it is marked in the same way. The number of rupture events decreases within the next 4.5 seconds to 11-12 per second and is even lower in the remaining time before solidification, namely 4/s. The film rupture events

recorded are not uniformly distributed in the sample but are more frequent on the r.h.s. of the image which is where the cold air hits the mould. The harsher cooling at this location therefore has a pronounced influence on cell wall ruptures. In conclusion, cooling has a visible impact on foam morphology but it cannot be held responsible for the characteristic shape of cell walls in solid aluminium foams. This already develops during foaming.

As the part produced in the experiments has slightly collapsed the result is not satisfactory under the viewpoint of foaming technology. The onset of cooling was too late and collapse of the foam triggered by contact with the hot mould walls. Recommendations for real production therefore include a temperature reduction shortly before mould filling, e.g., by turning off the heat source (if possible) or by turning on cooling earlier.

## 5 Summary and outlook

It was demonstrated that x-ray radioscopy is a suitable tool for visualising the foaming of aluminium alloys and to investigate problems of technological relevance. With the experimental possibilities now allowing to resolve the internal structure of expanding foams with spatial resolutions down to 10 μm and to obtain images frequencies up to 18 Hz the following conclusions could be drawn:

- A new processing route exploiting thixocasting of CIPped powder mixtures leads to an isotropic formation of bubbles avoiding the crack-like foaming behaviour with traditionally consolidated powders
- The expansion of metal foam is dominated by rupture processes of cell walls which take place whenever the thickness of the walls drops below about 50 μm. Rupture is a fast process taking less than 55 ms.
- Defects in the precursor material induce the local formation of voids but have little influence on the morphology of the fully expanded foam in the cases studied.
- Cooling of liquid foams induces local changes of foam morphology but the effect is quite limited and cannot be responsible for the overall structure of solid metal foam.

Future work should include, e.g., more in-depth investigations of the new processing route (II) by applying the radioscopic methods developed. Moreover, by increasing beam intensity one should be able to reduce exposure times to some milliseconds which would permit to capture images every 7-10 ms, thus allowing to obtain further improved estimates for the rupture time.

**Acknowledgement**s

The work was supported by Deutsche Forschungsgemeinschaft (programme SPP-1075, grant Ba 1170/3-2) and by the European Synchrotron Radiation Facility (ESRF). The authors would like to thank especially the team of beamline ID19, D. Fernandez-Carreiras, F. Thurel and P. Fajardo Sanz from the electronics support group. Help by Dirk Lehmhus is acknowledged who supplied a foaming mould.

## References

[1] J. Banhart, *Manufacture, characterisation and application of cellular metals and metal foams*, Prog. Mater. Sci. **46**, 559 (2001)

[2] J. Banhart, M.F. Ashby, N.A. Fleck (Editors), *Metal foams and porous metal structures*, MIT-Verlag, Bremen (1999)

[3] J. Banhart, M.F. Ashby, N.A. Fleck (Editors), *Cellular metals and metal foaming technology*, MIT-Verlag, Bremen (2001)

[4] M.F. Ashby, A.G. Evans, N.A. Fleck, L.J. Gibson, J.W. Hutchinson, H.N.G. Wadley, *Metal foams: a design guide*, Butterworth-Heinemann, Oxford (2000)

[5] B.T. Allen, M.W. Mote, A.M. Sabroff, US Patent 3087807 (1963)

[6] J. Baumeister, *Verfahren zur Herstellung poröser Metallkörper,* German Patent 40 18 360 (1990), see also US Patent 5,151,246 (1992)
[7] F. Baumgärtner, I. Duarte, J. Banhart, *Industrialisation of powder compact foaming process*, Adv. Eng. Mater. **2**, 168 (2000)
[8] A. Melzer, J. Banhart. J. Baumeister, M. Weber, *Verfahren zur Herstellung von Verbundwerkstoffbauteilen,* German Patent 198 13 176 (1998)
[9] V. Gergely, T.W. Clyne, *The FORMGRIP process: foaming of reinforced metals by gas release in precursors*, Adv. Eng. Mater. **2**, 175 (2000)
[10] I. Duarte, J. Banhart, *A study of aluminium foam formation - kinetics and microstructure*. Acta Mater. **48**, 2349 (2000)
[11] B. Kriszt, P. Cekan, K. Faure, *Foamability of the Al-Si system*, in Ref. [3], p. 77
[12] J. Banhart, H. Stanzick, L. Helfen, T. Baumbach, *Metal foam evolution studied by synchrotron radioscopy*, Appl. Phys. Lett. **78**, 1125 (2001)
[13] J. Banhart, H. Stanzick, L. Helfen, T. Baumbach, K. Nijhof, *Real-time observation of aluminium foam sandwich production by synchrotron radioscopy,* Adv. Eng. Mater. **3**, 407 (2001)
[14] F. Simančík, K. Behulová, L. Borš, *Effect of ambient pressure on metal foam expansion*, in Ref. [3], p.89
[15] L. Helfen, T. Baumbach, H. Stanzick, J. Banhart, A. Elmoutaouakkil, P. Cloetens, *Viewing the early stage of metal foam formation by computed tomography using synchrotron radiation*, Adv. Eng. Mater., this issue
[16] H.W. Seeliger, presentation at NIMR congress, Noorwijkerhout, 12.12.2001
[17] C. Körner, F. Berger, M. Arnold, C. Stadelmann, R.F. Singer, *Influence of processing conditions on morphology of metal foams produced from metal powder,* Mat. Sci. Tec. **16**, 781 (2000)
[18] B. Olurin, M. Arnold, C. Körner, R.F. Singer, *The investigation of morphometric parameters of aluminium foams using micro-computed tomography*, Mater. Sci. Engnr. **A328**, 334 (2002)
[19] A.E. Markaki, T.W. Clyne, *Characterisation of impact response of metallic foam / ceramic laminates*, Mat. Sci. Tec. **16**, 785 (2000)
[20] J. Banhart et al., unpublished data
[21] G. Lang, *Einfluß von Zusatzelementen auf die Oberflächenspannung von Reinstaluminium*, Aluminium **50**, 731 (1974)
[22] Product data sheet of *Alulight*®, Alulight GmbH Ranshofen, URL:www.alulight.com

Some of the x-ray movies described in this paper can be viewed and downloaded from web-site http://www.metalfoam.net/aem-movies.html.

## TABLES

**Table 1.** Cell wall thickness prior to rupture determined by analysis of x-ray radiographs. Note that although the pixel size was 10 μm, fractions of a pixel occur because the angle between pixel mesh and cell wall varied.

| frame interval (picture n → picture n+1) | cell wall thickness [μm] |
|---|---|
| **AlSi7 route I (sample II/63)** | |
| 52 → 53 | 50 (1st event)<br>70 (2nd event) |
| 54 → 55 | 55 |
| 79 → 80 | 54 |
| 83 → 84 | 58 |
| 91 → 92 | 62 |
| 109 → 110 | 38 |
| 134 → 135 | 58 |
| 178 → 179 | 40 |
| 98 → 99 | 38 |
| **Average** | **52 ± 11** |
| **AlSi6Cu4 route II (sample II/65)** | |
| 117 → 118 | 54 |
| 120 → 121 | 51 |
| 127 → 128 | 46 |
| 130 → 131 | 33 |
| 191 → 192 | 38 |
| 250 → 251 | 66 |
| 275 → 276 | 52 |
| 278 → 279 | 63 |
| 291 → 292 | 55 |
| 192 → 193 | 49 |
| **Average** | **51 ± 10** |

**Table 2.** Minimum cell wall thickness from various sources.

| **alloy** | **minimum thickness [μm]** | **source** |
|---|---|---|
| Al | 100 | [11] |
| AlSi2 | 80 | [11] |
| AlSi6Cu4 | 51 | this paper |
| AlSi7 | 52 | this paper |
| AlSi10 | 60-70 | [17]* |
| AlSi10Mg0.6 | 30-50 | [18]* |
| AlSi12 | 80 | [11] |
| AlSi12Mg0.6 | 60-80 | [19]* |

*estimate from a graphical representation

## FIGURES

**Figure 1**. Process steps for making foamable precursor material.

**Figure 2**. Experimental set-up for real-time radioscopy using a synchrotron beam.

**Figure 3**. Comparison of bubble formation in foams made by a) hot compaction of powders (route I) and b) thixocasting of CIPped powders (route II). In both cases an early expansion stage is shown: the volume expansion factor is 1.63 and 1.26 for route I and II, respectively.

**Figure 4.** Rupture of cell walls in metal foams; a) high resolution images (10 μm) separated by one frame (500 ms) in a AlSi7 foam (route I) and corresponding difference picture showing ruptured feature; b) analysis of cell wall thickness.

**Figure 5.** Idealised model of a rupturing cell wall used for estimating the time for film rupture.

**Figure 6.** Evolution of defects in AlSi7 foams visualised by x-ray radiographs. a) mica platelet, b) carbon fibres, c) lead oxide, d) steel washer, e) hole in precursor. All image series were taken at 2 Hz frequency and 40 μm resolution. Mould-free foaming was applied.

**Figure 7.** Evolution of a bulk of expanding granulated precursor material (AlSi7) inside a mould which was 10 mm thick in the beam direction and open to the top. Frame repetition frequency was 2 Hz, spatial resolution 40 μm.

**Figure 8**. Temperature course in solidification experiment. A AlSi7 foam was generated in a closed mould and quenched with cold air after the sample temperature had reached T=650°C. Image frequency is 2 Hz. Solidification and liquidification temperatures of AlSi7 are marked by dotted horizontal lines..

**Figure 9**. Foam images corresponding to solidification experiment described by **Figure 8**. a) x-ray radiographs, b) post-solidification image of a section of the foam. The circles in the third radiograph mark features which can be detected in the post-foaming section of the foam, where they are also marked. c) Rupture map showing changes in foam morphology from the moment cooling has been started (image #288) until solidification (image #350). Different grey scales denote different time and temperature intervals as defined.

# Figure 1

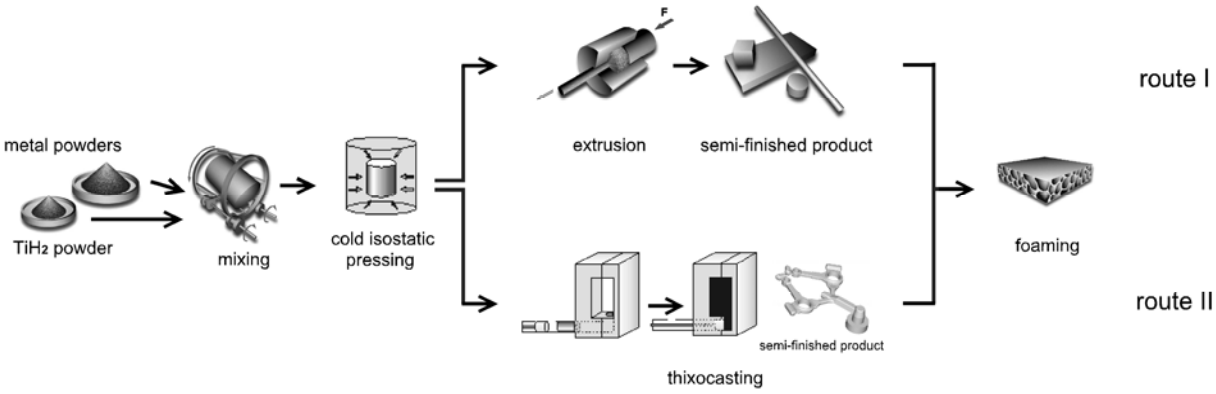


# Figure 2

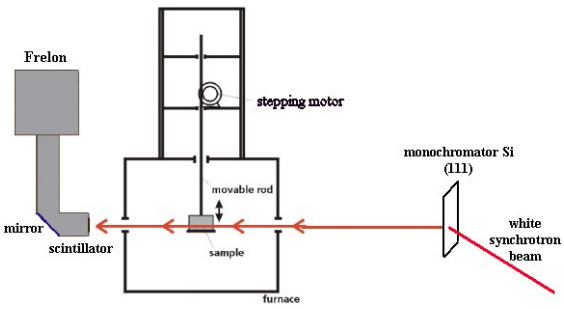


# Figure 3

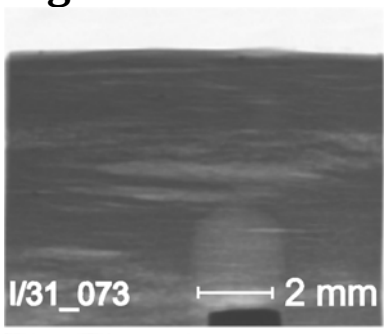


a)

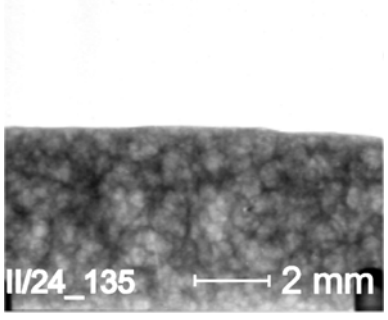


b)

# Figure 4

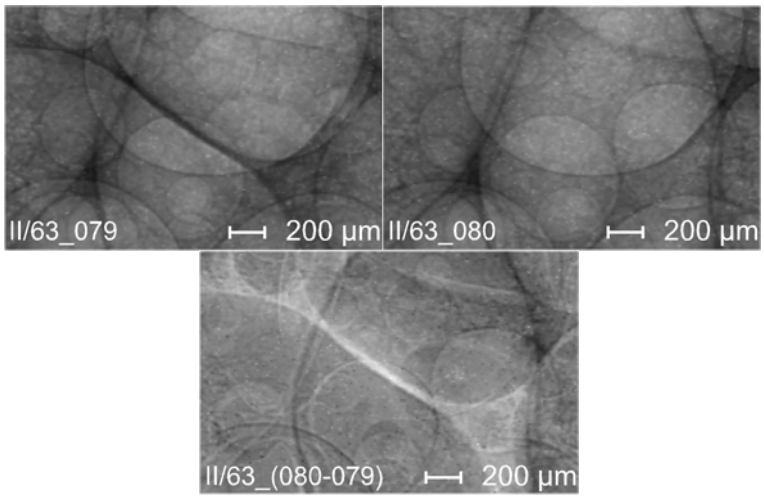


a)

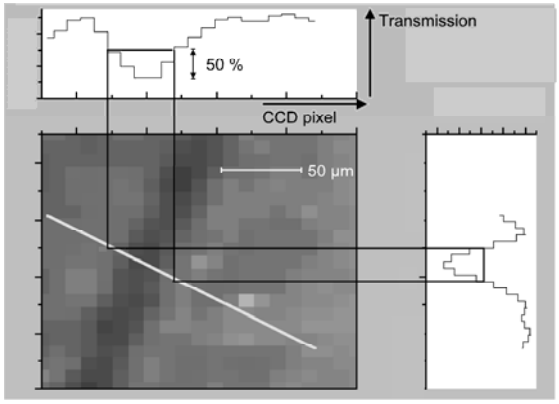


b)

# Figure 5

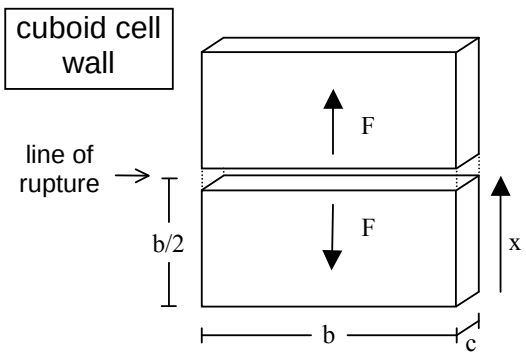

**Figure 6**


a)

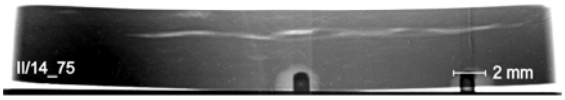


b)

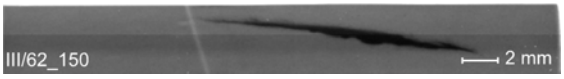


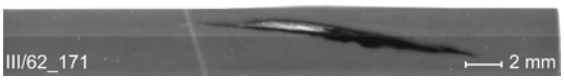


c)


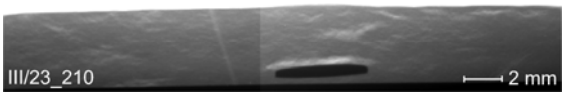


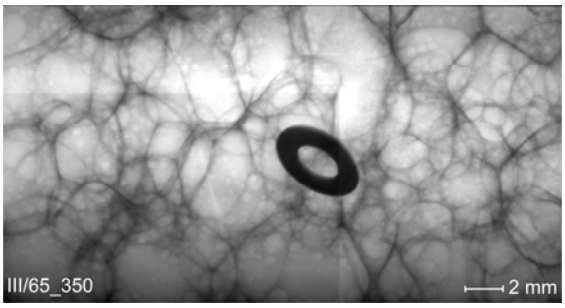


d)


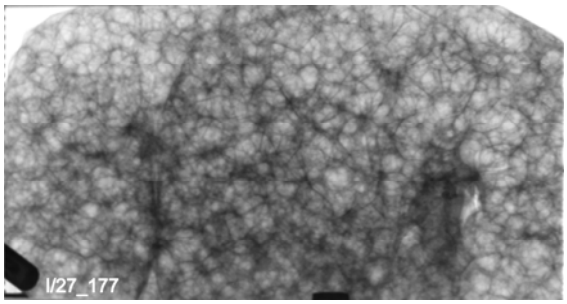


e)

# Figure 7

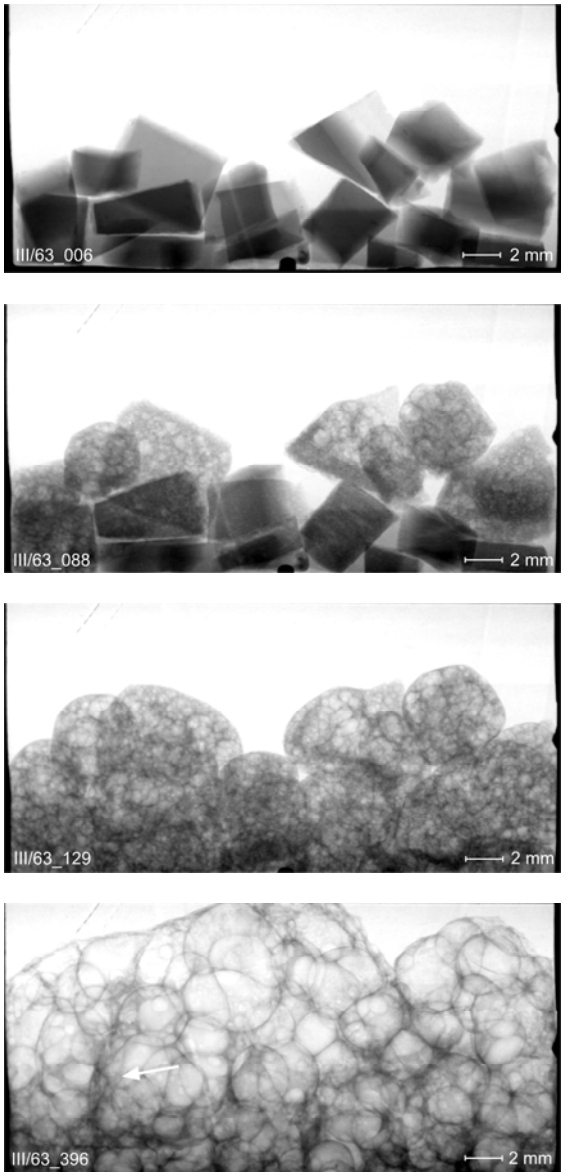


# Figure 8

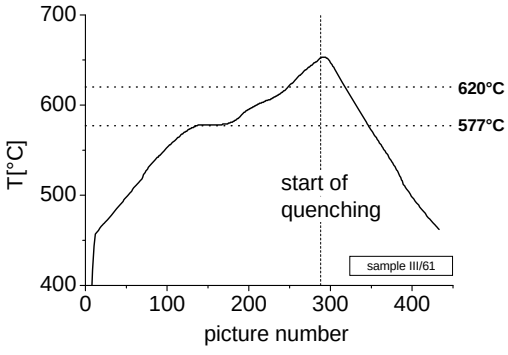

# Figure 9

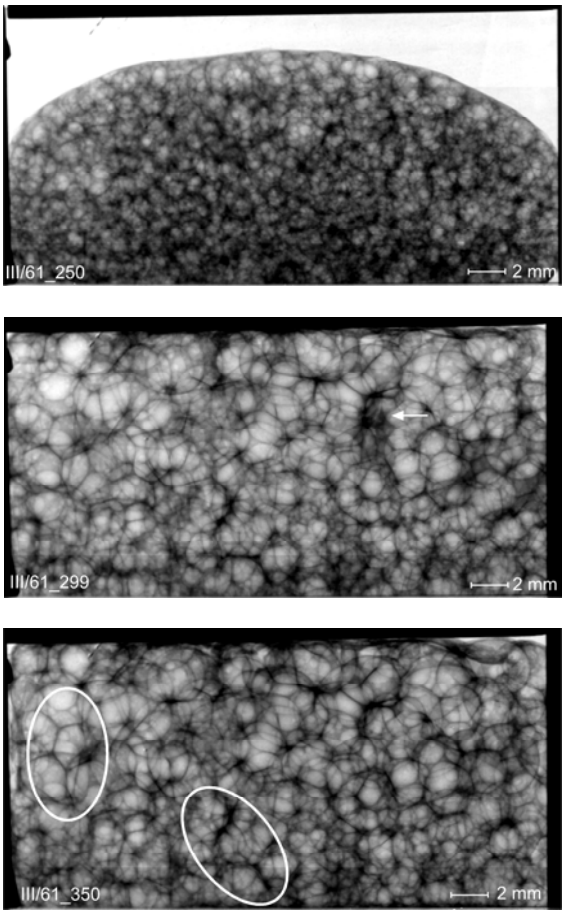
III/61_250
2 mm
III/61_299
2 mm
III/61_350
2 mm

a)

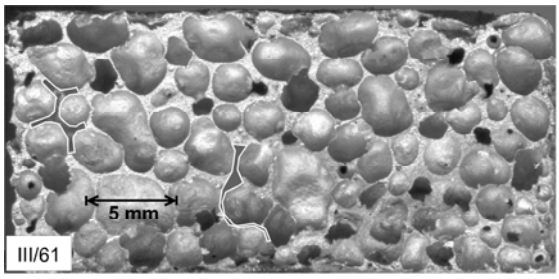
5 mm
III/61

b)

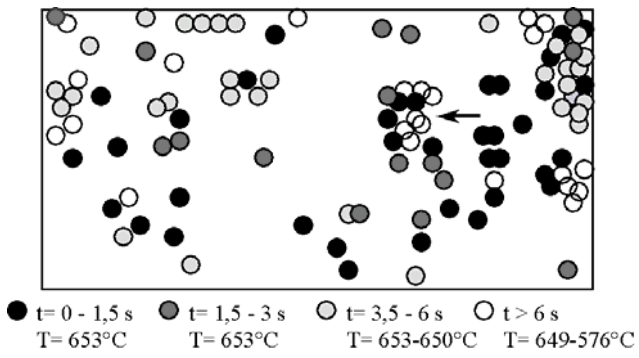
t= 0 - 1,5 s
T= 653°C
t= 1,5 - 3 s
T= 653°C
t= 3,5 - 6 s
T= 653-650°C
t > 6 s
T= 649-576°C

c)